River Flow 2010 - Dittrich, Koll, Aberle & Geisenhainer (eds) - © 2010 Bundesanstalt für Wasserbau ISBN 978-3-939230-00-7

Large eddy simulation of river flows

Wolfgang Rodi
Institute for Hydromechanics, Karlsruhe Institute of Technology, Karlsruhe, Germany

ABSTRACT: The paper gives a brief overview of experience gained so far with the application of the Large Eddy Simulation (LES) technique to river-related flows. A brief introduction is given to the LES technique in which the large-scale motion of turbulence in river flows is resolved by numerical solution of the time-dependent flow equations and only motions of scales smaller than the numerical mesh are modelled. Application examples are presented, ranging from relatively simple flows in open channels to geometrically complex flows close to those found in natural rivers and situations with dikes and groynes. The present capabilities and the future potential of LES for river flow calculations are discussed.

Keywords: Numerical simulation, River flow, Turbulence, Eddies, Vortices

1 INTRODUCTION

The flow in rivers is always turbulent and the turbulent fluctuations contribute significantly to the transport of momentum, heat and mass. Even in the simplest variant of flow in a straight, smooth channel the turbulence generated near the bed is highly complex, featuring a variety of three-dimensional coherent structures (Nezu and Nakagawa 1983). The turbulence is complicated even further by geometrical variations such as due to bed forms, roughness elements and vegetation, changes in river cross-section, bends causing secondary motions, confluences associated with strong shear layers and all kinds of man-made structures such as dikes, bridge piers, groynes etc. In cases with abrupt changes in geometry the flow separates and large-scale structures and extensive vortices, often involving unsteady shedding, develop. In shallow river flow these vortices, especially those behind structures, often comprise mainly a horizontal two-dimensional motion, but in the vicinity of the structures they are mostly highly three-dimensional.

The turbulent fluctuating motion has a strong influence on the overall flow development due to increased bed friction and hence on the discharge and water elevation. It also governs the sediment transport and local forces on boundaries and dilution of contaminants. Here the large-scale turbulent structures are particularly effective.

In river engineering there is a great need for predicting all these features and phenomena of practical importance, and there is also a need for understanding better the details of the turbulent processes. At present, calculations in practice are still carried out with so-called RANS methods, in which Reynolds-averaged equations for mean-flow quantities are solved, i.e. the turbulence is averaged out and its effect has to be accounted for entirely by a RANS turbulence model. Most models in use employ the eddy viscosity /diffusivity concept and estimate the eddy viscosity through simple algebraic relations or model transport equations such as in the k-ε turbulence model. These RANS methods are economical and on modern computers can cover larger regions and river stretches, especially when 2D depth- averaged versions are employed. However, many of the phenomena cited above cannot be accounted for adequately, especially when larger-scale structures play a dominant role for the transport of momentum, heat and mass or when details of the flow, such as unsteady processes like vortex shedding and unsteady forces on structures or bed elements, are important and need to be resolved. A tool more powerful to solve these problems, the Large-Eddy Simulation (LES) technique, evolved recently which, like in

other fields of fluid mechanics, is also used more and more in river flow calculations. LES is a method in between RANS mentioned above and Direct Numerical Simulation (DNS); the latter solves numerically the exact 3D time-dependent Navier-Stokes equations without any model, thereby resolving all scales of the turbulent motion from the large ones down to the smallest, dissipative scales. As the size of the smallest scales relative to the extent of the flow domain decreases linearly with the Reynolds number (Re), the number of grid points necessary for resolving all motions in a 3D calculation increases roughly with Re^3. As a consequence, for Re of practical relevance the number of grid points required becomes so large that the computational effort exceeds by far the capabilities of even the biggest available computers. Therefore DNS is not a method for practical calculations, but it is a very useful tool for fundamental research.

The method in between RANS and DNS, the Large Eddy Simulation (LES), also solves the 3D time-dependent flow equations, but determines thereby only those turbulent motions that can be resolved on a given numerical grid (see Figure 1), i.e. motions with scales larger than the grid size, and accounts for the effect of the sub-grid-scale (SGS) motions that cannot be resolved by a SGS model. This effect is mainly dissipative and in some methods is alternatively achieved by using a numerical scheme introducing some numerical dissipation. Away from walls, the larger turbulent eddies containing most of the energy and contributing most to the momentum, heat and mass transfer are virtually independent of Re, so that in this area LES does not have a Reynolds number problem. However, near walls the length scale of turbulence decreases with increasing Re so that the number of grid points required to resolve the near-wall zone adequately increases approximately with Re^2. Again, such calculations require so much computing effort that they are not possible at the high Re occurring in practice. Hence, in order to apply LES, special near-wall modelling is necessary. One possibility is to use wall functions bridging the viscous sub-layer, another is the use of RANS modelling in the near-wall zone as in the Detached Eddy Simulation (DES) approach first proposed by Spalart et al. (1997). In the present paper, examples of Large Eddy Simulations and also some DES of river flow situations are presented and discussed. The method itself is introduced only briefly as this is covered well in previous publications (e.g. Piomelli and Chasnov 1996, Fröhlich and Rodi 2002). Also, only genuine LES, which is always 3D, is covered in this paper. For shallow river flows, 2D depth-averaged LES methods have been developed and used (also sometimes called depth-averaged URANS) that resolve only the large-scale horizontal turbulent motions while the effect of the smaller-scale, bottom-generated turbulence needs to be modelled (sub-depth-scale model). This more economic approach is dealt with in Hinterberger et al. (2007) and was found to be less accurate and less realistic in providing details.

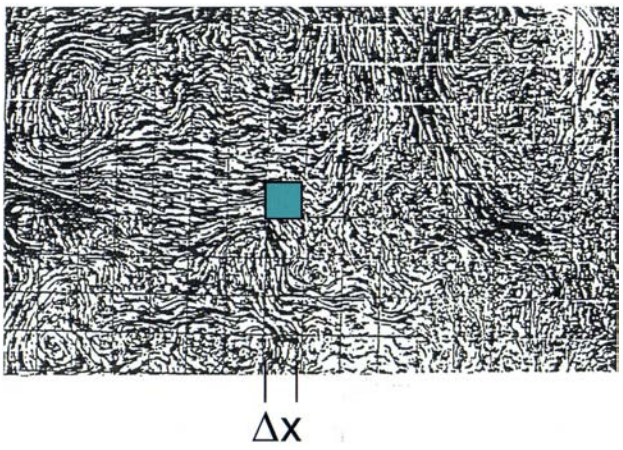

Figure 1. Turbulence on surface of a stirred tank with grid showing a control volume

2 LES METHODOLOGY

In LES of river flows, the filtered incompressible 3D Navier-Stokes and continuity equations are solved. The filter width is determined by the grid size so that the filtering removes the small-scale motions that cannot be resolved on a given grid, so that the resolved quantities are basically averages over the control volumes formed by the numerical mesh as illustrated in Figure 1 for turbulence in a stirred tank made visible by surface floats. Due to the non-linearity of the Navier-Stokes equations, the averaging introduces sub-grid-scale (SGS) stresses representing the effect of the small-scale unresolved turbulent motion on the resolved motion. A SGS model needs to be introduced for these stresses, and in analogy to modelling of the Reynold stresses in RANS methods, mostly a SGS eddy viscosity ν_t is introduced, which itself has to be determined from a model. In the applications presented in this paper, the SGS eddy viscosity is either determined with the original Smagorinsky model relating it to the strain rate of the resolved motion and to the average mesh size using a constant coefficient. Alternatively, a dynamic version of this model is used in which the coefficient is determined locally and instantaneously from the information available from the smallest resolved scales (Germano et al., 1991). With an eddy viscosity ν_t used for determining the SGS stresses, the flow equations solved in a LES are the same as those in an

unsteady RANS (URANS) calculation, only the model for determining ν_t is different: in URANS it relates ν_t exclusively to geometrical parameters (e.g. water depth h) and physical quantities (e.g. friction velocity U_τ, turbulent kinetic energy k, dissipation rate ε), while in LES ν_t is related to and hence determined by the mesh size, resulting in much lower eddy viscosities and, when the grid is refined more and more, ν_t goes to zero so that the LES turns into a DNS.

For heat and mass transfer problems, the equivalent filtered equations for scalar quantities are solved by LES and the sub-grid-scale fluxes appearing in the filtered equations are again determined by an SGS model, mostly introducing an eddy diffusivity which is normally set proportional to the SGS eddy viscosity.

The filtered equations are solved numerically, in the examples presented with Finite-Volume methods of various origins and types. When sub-grid scale models are employed as in the examples presented, it is important that little numerical dissipation is introduced and hence usually central differencing is employed for discretizing the convection terms. There is, however, a school propagating so-called implicit LES (ILES) where no SGS model is used but its (mainly dissipative) effect is left to the numerical dissipation introduced by methods employing upwinding (e.g. Fureby and Grinstein 1999).

2.1 *Near-wall treatment and boundary conditions*

As was mentioned already, at high Reynolds numbers well resolved LES near walls is not affordable so that special measures need to be taken in this case. One possibility is to bridge the viscous sub-layer in direct proximity to walls by wall functions, basically relating the resolved velocity at the first grid point away from the wall by logarithmic or exponential profile assumptions to the friction velocity. This is also the easiest method to account for wall roughness which is important in river flow calculations. An alternative is to use RANS modeling in the near-wall zone and switch to LES only somewhat away from the wall, an approach adopted in the Detached Eddy Simulation – DES (for a review see Spalart 2009) – a method applied in two of the examples presented below.

Another boundary of the calculation domain in river-flow calculations is the free surface – here in the examples presented the rigid-lid approximation is used. In this, the actual surface elevations are suppressed and their effects are simulated via pressure variations, i.e. pressure gradients at the boundary. This is a workable approximation when the actual surface deviation from the mean represented by the fixed frictionless lid is small, as should be the extent of the calculation domain.

The specification of conditions at inflow boundaries is considerably more difficult and elaborate than in RANS calculations since in LES realistic fluctuations must be provided at the inflow boundary. No problem arises when the flow is periodic in the streamwise direction, as is the case in some examples presented below, so that periodic conditions can be applied. Otherwise precursor calculations of a simplified situation (normally developed channel flow) must be performed to provide inflow fluctuations, or turbulence must be generated synthetically and super-imposed on a guessed or measured velocity distribution at the inflow. At the outflow, generally the convective boundary condition is used which allows disturbances to leave the domain freely.

3 EXAMPLES OF LES CALCULATIONS

In the following sections, examples of LES of some river flow situations are presented, moving from simple channel flow to geometrically more complex situations. The results shown are taken from publications, where all the details of the calculations are described, and concentrate on fluctuations and turbulence structures resolved by the LES.

3.1 *Developed straight open channel flow*

The first example taken from Hinterberger et al. (2008) concerns developed flow in a straight open channel with smooth walls at a Reynolds number based on friction velocity U_τ and channel depth h of $Re_\tau = 590$ (Re_h based on h and bulk velocity is 11000). The channel is considered infinitely wide and the flow developed and hence periodic boundary conditions were applied in both streamwise and spanwise direction. The LES was carried out with the standard Smagorinsky SGS model, but with near-wall damping of ν_t. The numerical grid had 8 Mio points and the wall-parallel resolution was in wall units $\Delta x^+ = 29$ and $\Delta y^+ = 14.5$ in streamwise and spanwise direction, respectively. The first grid point had a distance of $z_p^+ = 1.5$ from the bed. Hence, the conditions for a well-resolved LES were satisfied and no special near-wall treatment was necessary. In Figure 2 (left) calculated distributions over the depth of mean velocity and RMS values of the fluctuating components and of the shear stress $\langle u'w' \rangle$ are compared with DNS results of Moser et al. (1999) for closed channel flow at the same Re_τ (based on channel half width). The agreement can be seen to

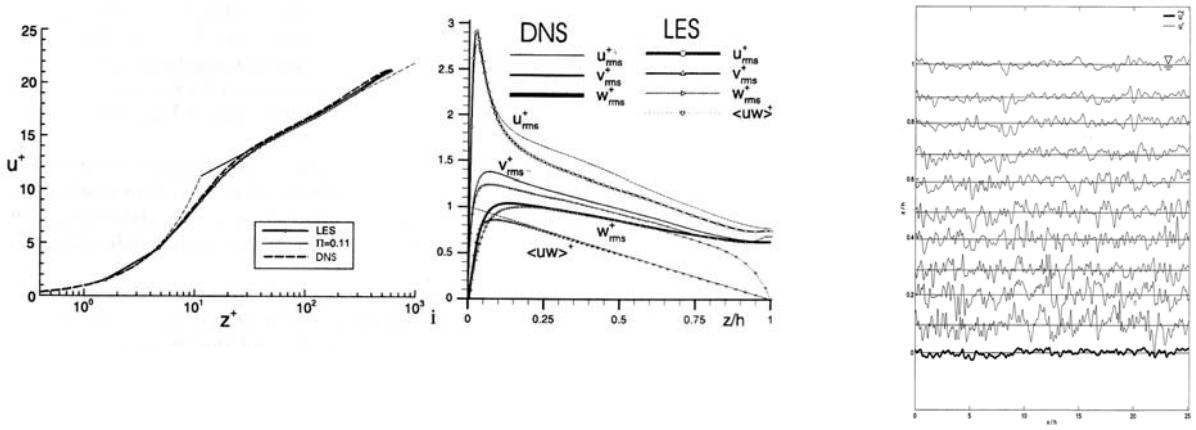

Figure 2. Flow in straight open channel with $Re_\tau = 590$ (from Hinterberger et al. 2008);left: distribution of mean velocity and fluctuating components;right: streamwise variation of u-fluctuations at various depths for one instant in time.

be good, but it should be noted that near *z/h = 1* the normal fluctuations are damped by the free-surface boundary while in the DNS this location is in the middle of the closed channel. The LES distributions agree also fairly well with measurements of Nezu and Rodi (1986). Figure 2 (right) gives evidence of the resolution of turbulent fluctuations by the LES. The figure shows for one instant in time the streamwise distribution of u-fluctuations at different depths z/h. As was to be expected from the RMS profile, the fluctuation amplitude is highest near the bed and decreases monotonically towards the free surface. Also, near the bed high frequency fluctuations (corresponding to small-scale turbulence) can be seen to be superimposed on lower frequency fluctuations. Near the surface, the high frequency fluctuations are absent and the motion consists only of larger scales. In Hinterberger et al. (2008) spectra are provided which support these findings quantitatively. The lowest, thick-line signal in Figure 2 (right) represents the instantaneous depth-averaged u-fluctuations, showing clearly that also the depth-averaged velocity field carries fluctuations which a realistic 2D depth-averaged LES would have to yield. As the LES has near-DNS resolution near the wall, the same turbulence structures as obtained by DNS, with streaks, sweeps, and ejections, are also produced by the LES.

3.2 *Flow over 2D periodic dunes*

The next example concerns the flow in a wide open channel with the bed consisting of periodic dunes as calculated by Stoesser et al. (2008). The ratio of dune wave-length λ to dune height k is 20 and the ratio of λ to water depth h is 5. Re based on h and bulk velocity is 25000. The computational domain spanned 1 dune length λ in the fluctuations behave differently, as in the LES the streamwise and 8 k in the spanwise direction, and periodic boundary conditions were applied in both directions. The numerical grid had about 9 Mio points and the resolution was again good enough so that no special near-wall modelling was necessary. In this LES, the dynamic version of the Smagorinsky SGS model was used. The mean velocity field and the streamwise and wall-normal turbulent intensities and the Reynolds shear stress calculated by the LES agree well with experiments of Polatel (2006). Figure 3 shows examples of the instantaneous flow field and the coherent structures resulting from the LES. The flow separates near the dune crest and spanwise vortices (or rollers) develop in the separated shear layer springing off the crest. These rollers grow and are swept downstream along the stoss side of the following dune and are lifted upward by the boundary layer redeveloping on this side (Figure 3a). They reach the surface where they break up in a boil. The upward motion appears to be associated with hairpin vortices whose lines are bent upwards so that the structures carry vertical vorticity. This leads to the fluctuating surface motion shown in Figure 3b. At reattachment and somewhat beyond, the rollers, which have been broken up already by spanwise instabilities, impinge on the dune wall (Figure 3c) where they cause locally high turbulence and a reorientation of impinging fluid in directions tangential to the wall (splatting effect). All the complex and important details of the turbulent motion are produced realistically by the LES and can be studied from its results.

3.3 *Open channel flow over permeable bed*

Some results are presented here of the LES carried out by Stoesser et al. (2007) of flow in an open

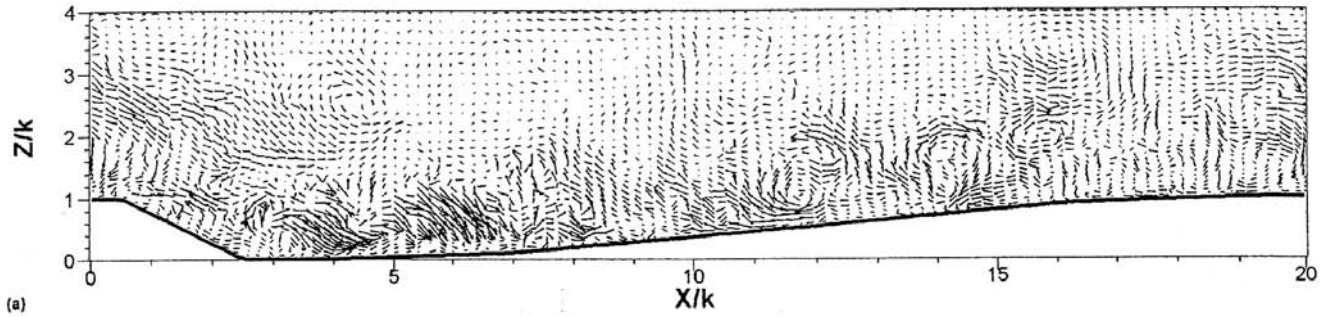

a) instantaneous velocity perturbations in a longitudinal plane

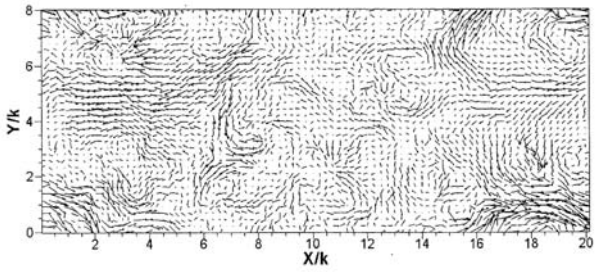

b) snapshot of instantaneous velocity perturbations near surface

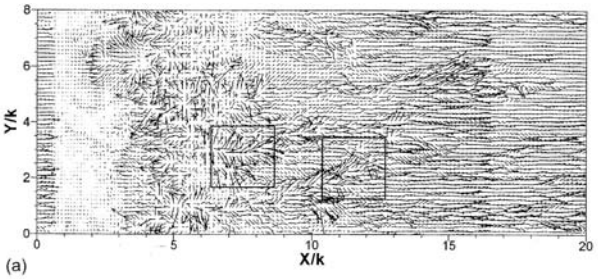

c) snapshot of instantaneous velocity vectors near bed

Figure 3. Flow over 2D periodic dunes (from Stoesser et al. 2008)

channel over and through 3 layers of spheres. Here the roughness effect of the spheres was investigated as well as the interaction of the turbulent flow in the channel and in the pores between the spheres. The flow configuration was chosen according to the experiments of Prokcrajac (2005) with a water-depth-to-sphere diameter ratio *of h/d = 3.42* and a Reynolds number of $Re = Uh/\nu = 15200$. The calculation domain of the surface-flow region spanned 5.3 h × 5.3 h × h and the subsurface region consisted of 3 layers of spheres of diameter d arranged in a cubical pattern with 18 × 12 spheres per layer. Periodic boundary conditions were applied in both streamwise and spanwise direction. 75 Mio grid points were used, with 40 points over each sphere diameter, and the near-wall resolution allowed again a well-resolved LES without any special modelling in this region. As SGS model, the dynamic Smagorinsky model was employed. The calculated mean-velocity distribution in the surface flow was found to agree well with the measured one, and the calculated turbulent intensities indicate that considerable turbulence intrudes into the subsurface area with the high wall-normal fluctuations in the interface region causing high mass and momentum exchange.

Figure 4 gives a snapshot of the complex velocity perturbation field providing insight into the turbulent structures prevailing. At the time instant shown there are strong ejections away from the interface while at other instants sweeps towards the interface were observed. The LES allow to study the instantaneous forces acting on the individual spheres and hence also the mechanisms causing erosion of sediment particles from the bed.

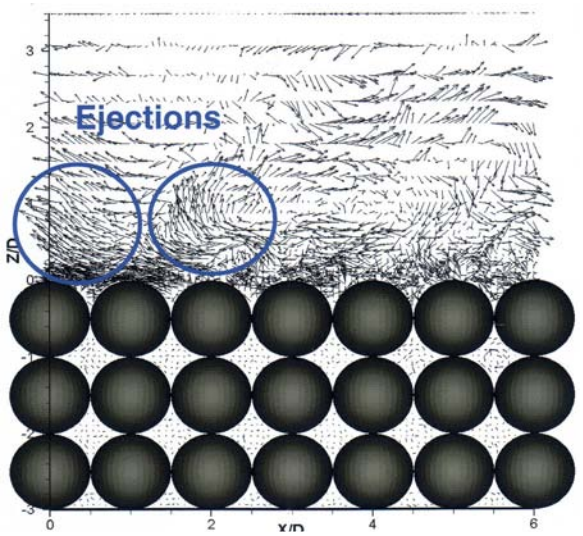

Figure 4. Open channel flow over 3 layers of spheres; snapshot of perturbation velocity vectors in plane through centre of spheres (from Stoesser et al.. 2007)

3.4 *Flow in strongly curved open channel*

Results are now presented from the DES carried out by Constantinescu et al. (2010) of flow in an open channel bend of high curvature over realistic topography (see Figure 5a) corresponding to equilibrium scour conditions. Blanckaert (2002) had carried out a mobile-bed experiment of such a

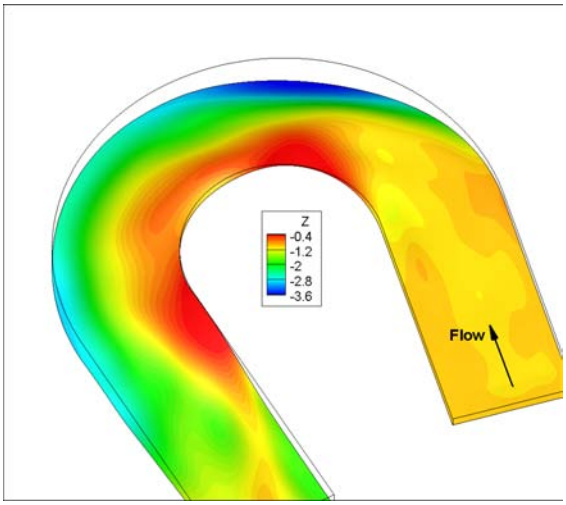

a) Bed geometry and bathymetry

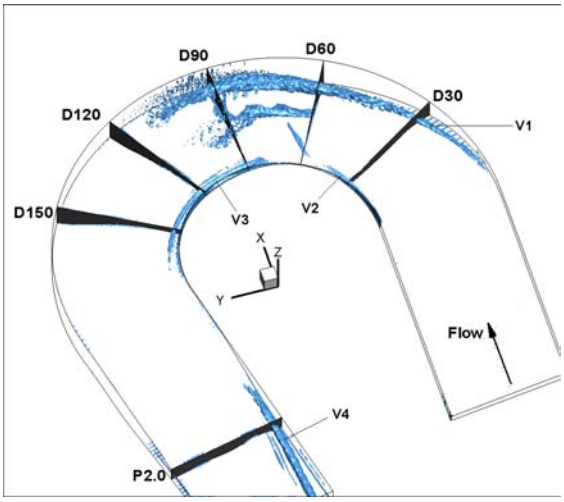

b) Predicted vortical structures of mean flow visualized by Q criterion

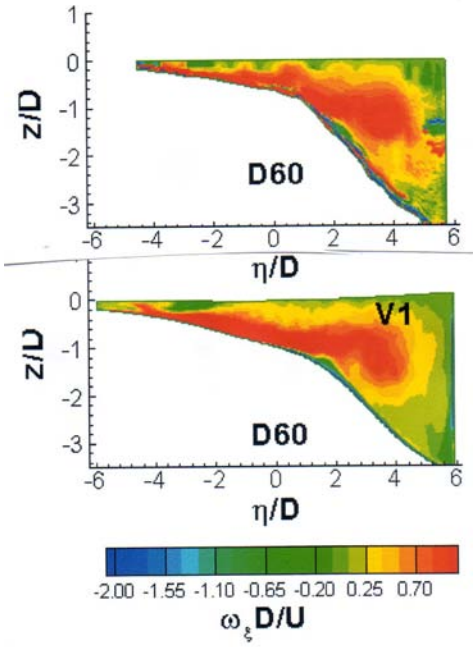

c) Mean-flow streamwise vorticity in section D60; top: experiment, bottom: DES

Figure 5. Flow in strongly curved open-channel bend (from Constantinescu et al. 2010)

bend flow and measured the bathymetry and velocity after the flow and sediment transport had reached equilibrium. This situation, with the topography fixed, was calculated by the DES method of Spalart et al. (1997) using as base model the Spalart-Allmaras (SA) one-equation turbulence model. The Reynolds number based on flume-averaged depth and velocity is 68400. The calculation domain extended to 7 channel widths upstream of the bend entrance. Inflow conditions were generated by a precursor DES of developed straight channel flow. In the main computation domain, 10 Mio grid cells were used and grid spacing in the wall-normal direction was quite fine, but in the wall-tangential directions the spacing was not fine enough for a well resolved LES. Hence, near the wall the equations were solved with the SA model in RANS mode. The DES yielded reasonably good agreement with the measurements for streamwise velocity and the secondary motion. For a cross-section 60° from the bend entrance the latter is illustrated in Figure 5c by the streamwise vorticity. Figure 5b visualizes various vortices in the bend as predicted by the DES. The vortex V1 corresponds to the main cross-stream circulation developing in the outer half of the cross-section. There are 3 also streamwise oriented vortices V2, V3, and V4 in the vicinity of the inner bank while the vortex in the middle halfway around the bend, which is associated with the shear layer forming on the outside of the point bar, is more vertically oriented. This calculation example demonstrates that geometrically complex river-flow situations as they occur in nature can be calculated realistically by LES (here by its DES variant).

3.5 *Flow structures at river confluence*

The next example concerns a DES study of the flow at the confluence of the Kaskaskia River and the Copper Slough stream in Illinois, USA, taken from Miyawaki et al. (2010). The flow and geometrical parameters in the DES were close to those in 2 field studies by Rhoads and Sukhodolov (2001, 2008). The first study (case 1) was for a momentum ratio Mr ≈ 1 and a Reynolds number Re based on mean values of velocity and flow depth of 166 000 and the second (case 2) for Mr ≈ 5 and Re = 77 000. In a separate paper (Miyawaki et al. 2009), the DES method was validated with the field data for case 1. The results presented here will concentrate on the flow structures predicted by DES for the 2 cases. The DES method and the generation of inflow conditions were the same as in the previous example (bend flow) and 5 Mio grid prints were used. The bathymetry was non-uniform and is included in Figure 6(ii).

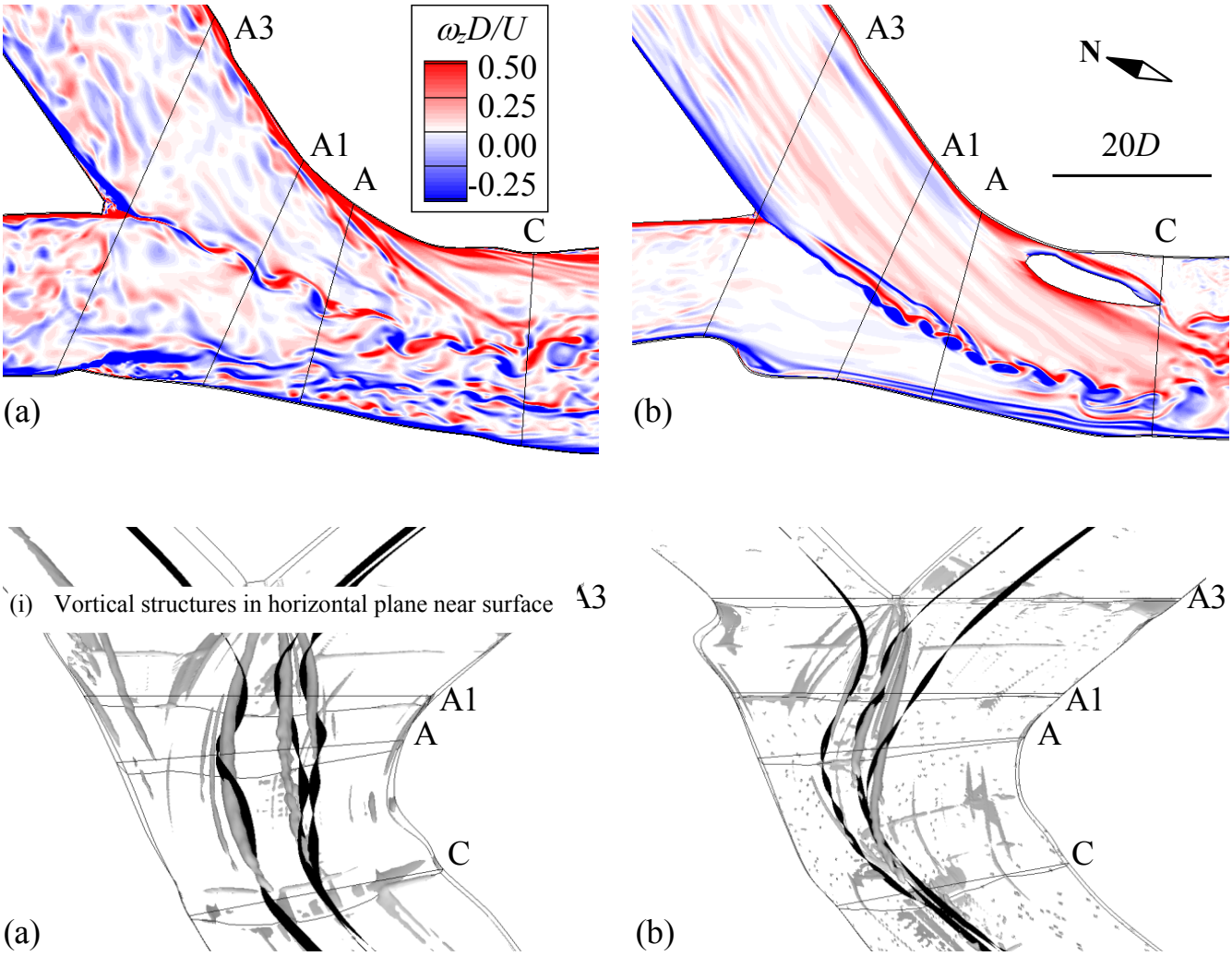

(ii) Streamwise oriented vortices visualized by Q-criterion

Figure 6. Flow structures at river confluence for 2 momentum ratios M_r (left $M_r \approx 1$, right $M_r \approx 5$; from Miyawaki et al. 2010)

For the 2 momentum-ratio cases, the vortices developing in the mixing layer between the 2 confluence streams is shown in Figure 6(i). Significant differences can be seen which are discussed in detail in Miyawaki et al. (2010). Here, attention is drawn only to the observation that in case 1 with little velocity difference between the merging streams the vortices in the mixing layer are like in a van Karman vortex street with alternating rotation. On the other hand, in case 2 with significant velocity difference the vortices are driven by a Kelvin-Helmholtz instability and exhibit only clockwise rotation. Figure 6(ii) displays the streamwise oriented vortices (grey) that are generated at a confluence, with 3D ribbons (black) added to indicate the sense of rotation. A complex system of such vortices develops with also significant differences between the 2 cases. In case 1 it is mainly these vortices and not the ones in the mixing layer that cause the mixing of mass in the cross-stream direction. This calculation example also shows convincingly that LES (here DES variant) can provide information on all the essential flow structures in complex real-life situations.

3.6 *Flow around a spur dike in an open channel*

In this section some exemplary results are shown from the LES of Koken and Constantinescu (2008) of the flow around a spur dike placed in an open channel. Geometry and computational domain are given in Figure 7(i) together with the bathymetry. As in the channel-bend example, the bathymetry was taken from a loose-bed experiment (performed also by the authors) and corresponds to equilibrium scour conditions. The Reynolds number was fairly low ($Re = UD/\nu = 18000$) so that with 4 Mio cells the grid was fine enough near the walls for a well-resolved LES and hence there was no need for special near-wall modelling. The dynamic Smagorinsky SGS model was employed and the inflow conditions were generated by a precursor LES of developed channel flow. A very complex 3D flow develops around the spur dike, with separation regions in front and behind the

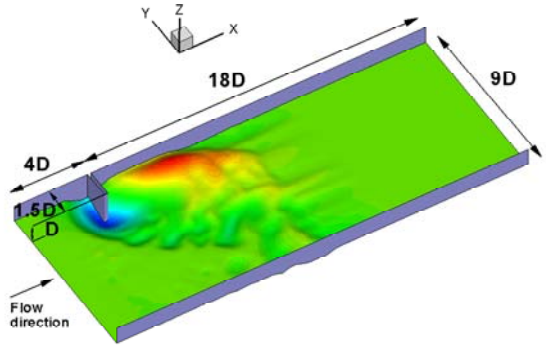

(i) Flow geometry, computational domain and bathymetry

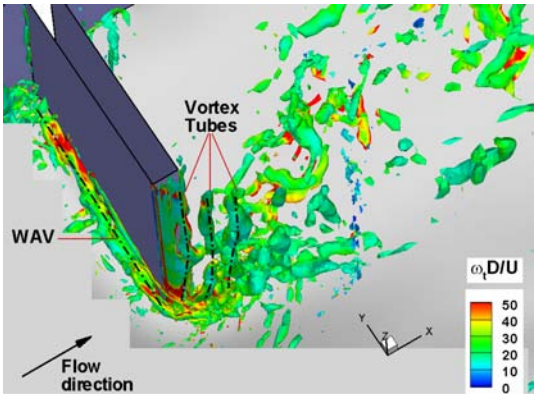

(ii) Coherent structures visualized by Q-criterion

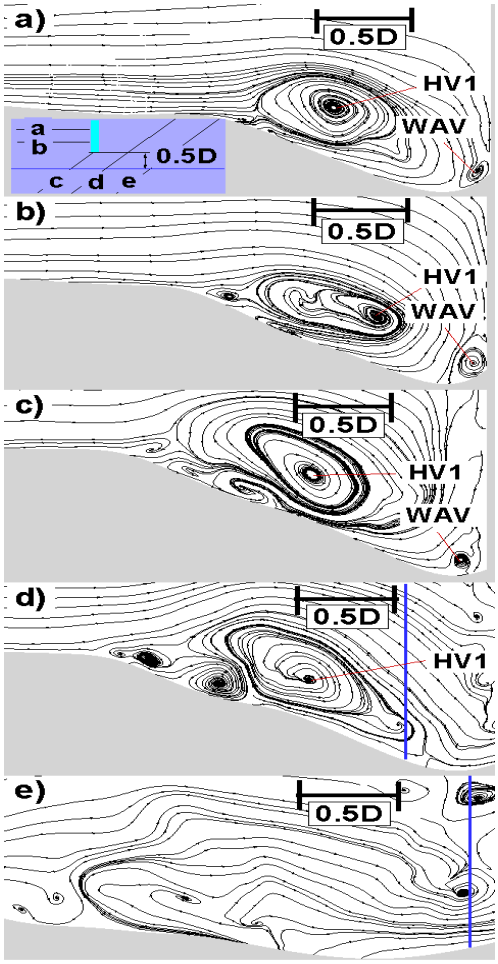

(iii) Instantaneous 2D streamlines in various vertical planes (see inset in figure part a) near spur dike

Figure 7. Flow around a spur dike in an open channel (from Koken and Constantinescu 2008)

dike, the former being the origin of the horseshoe vortex near the bed and the latter associated with a detached shear layer formed by shed vortices. Figure 7(ii) shows a 3D snapshot of these structures. The horseshoe vortex system is illustrated by 2D instantaneous streamlines in Figure 7(iii) and shows a large primary necklace, which was found to undergo bimodal oscillations, and smaller upstream-located secondary and tertiary vortices. The scour hole in front of the dike was found to influence strongly the development of the horseshoe vortex system. Koken and Constantinescu (2008) also present distributions of mean and instantaneous bed friction and exploit their LES results for a detailed discussion of the scour mechanisms.

3.7 *Flow and mass exchange in groyne field*

Hinterberger et al. (2007) used LES to simulate the flow and tracer concentration in a groyne field that was studied experimentally by Weitbrecht et al. (2008). The latter authors placed a series of 15 groynes in a flume and measured the surface flow by PIV and also the temporal development of tracer concentration in one groyne field initially seeded by uniform tracer concentration. Because of periodic behaviour of the flume in the most downstream located groynes in the series, only one groyne field was computed in the LES and periodic boundary conditions were applied in the downstream direction, the computation domain extending from the middle of one groyne field to the middle of the next one. In the situation simulated, the ratio of groyne length to groyne distance was W/h = 0.4, the ratio of groyne length to water depth W/h = 10.8 and the Reynolds number Re = Uh/ν = 7340. The standard Smagorinsky SGS model was used and the grid having 3 Mio points was not fine enough for a well-resolved LES so that wall functions were employed at all walls. The main recirculation flow in the groyne field was well predicted, but the secondary recirculation in the lee of the upstream groyne was underpredicted compared with the experiments, particularly near the surface.

The instantaneous flow field exhibiting vortices in the separated shear layer between the tips of the groynes is simulated in good accord with the experiment, as can be seen from the snapshots in

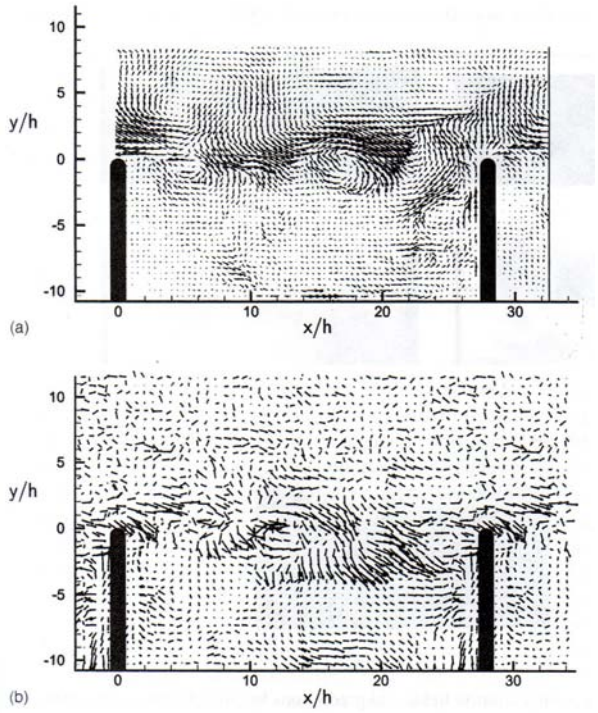

Snapshot of instantaneous perturbation velocityvectors at surface (top: experiment, bottom: 3D LES

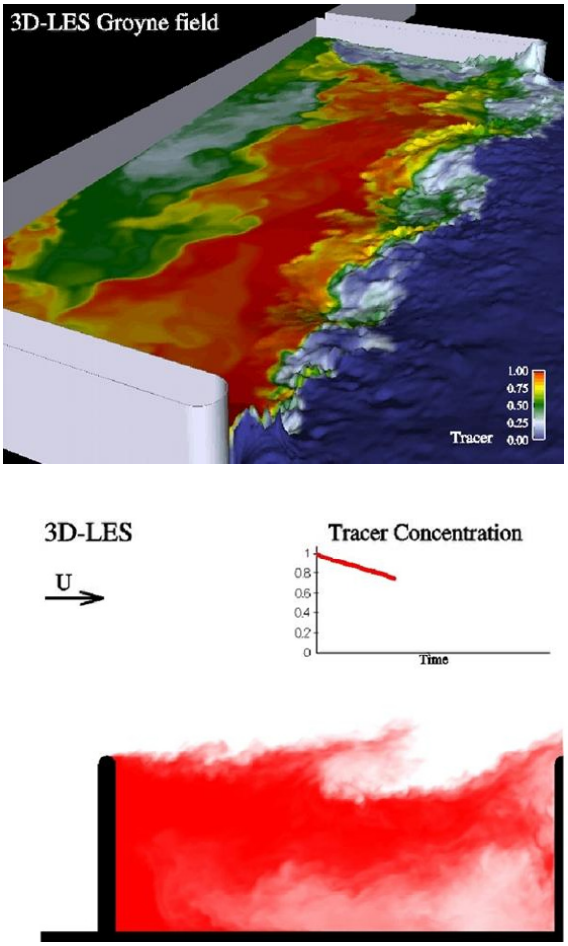

Snapshot of washing out of tracer (top: at surface; bottom: depth-averaged tracer field)

Figure 8. Flow and mass exchange in a groyne field (from Hinterberger et al. 2007)

Figure 8 (left). These vortices can also be seen clearly in Figure 8 (right) which shows snapshots of the concentration field some time after the start of washing out of a tracer from the groyne field by the turbulent mass exchange processes. The top figure is a snapshot of contours of the surface tracer concentration and also of the surface elevation (calculated from the pressure distribution at the frictionless rigid lid representing the free surface). The lower figure displays the depth-averaged concentration, visualizing nicely the large-scale structures that are most effective for the mass exchange. The inset shows the decay with time of the average concentration in the groyne field.

4 CONCLUSIONS

In this paper it was shown that the Large-Eddy Simulation method can be applied to river flow problems and allows to predict and study situations with particularly complex flow behaviour. The method not only yields information on complex mean-flow features but also on unsteady features by resolving the large-scale eddies of the turbulent motion. LES is clearly superior to RANS whenever large-scale structures dominate the flow and scalar-transport behaviour and when unsteady processes like vortex shedding and fluctuating forces need to be determined. The details that can be obtained from a LES are important for furthering our understanding of the physical mechanisms, e.g. the ones responsible for the scour process. The next step would then be to add a model for the sediment transport and to calculate the development of a mobile bed by LES.

The 3D time-dependent LES calculations are expensive, but they are affordable on modern high-performance computers and increasingly on clusters of PCs. However, well-resolved LES are feasible only for problems with relatively low Reynolds numbers. At high Reynolds numbers, as they are usually found in practice, the near-wall region cannot be resolved at reasonable cost. Calculating this sub-region with a RANS model, such as in the Detached-Eddy Simulation (DES) technique, appears to be the most promising solution to overcome this problem and hence

Hybrid RANS/LES methods of this type will be the methods for practical application. Another type of hybrid method is also promising, namely Embedded LES: the expensive LES is applied only in sub-regions of the calculation domain where the flow is particularly complex and not amenable to RANS, such as in the vicinity of structures; the main part of the domain, where RANS yields results of sufficient accuracy for practical purposes, is calculated with this much cheaper method. Finally, there is a clear trend that, because available computer power will continue to increase, LES and particularly its hybrid variants will soon be used also for practical river-flow calculations.

ACKNOWLEDGEMENTS

The author is grateful to G. Constantinescu for providing figures of his results.

REFERENCES

Blanckaert, K. 2002. Flow and turbulence in sharp open-channel bends. PhD thesis No. 2545, Ecole Polytechnique Fédérale, Lausanne, Switzerland.

Constantinescu, G., Koken, M., Zeng, J. 2010. Simulation of flow in an open channel bend of strong curvature using detached eddy simulation. Proc. River Flow 2010, Braunschweig, Germany.

Fröhlich, J., Rodi, W. 2002. Introduction to Large Eddy Simulation of turbulent flows, in: Closure strategies for turbulent and transitional flows, B.E. Launder and N. Sandham, eds. Cambridge University Press, 267-298.

Fureby, C., Grinstein, F. 1999. Monotonically integrated Large-Eddy Simulation of free shear flows. AIAA J., 37, 544-556.

Germano, M., Piomelli, U., Moin, P., Cabot, W.H. 1991. A dynamic sub-grid scale eddy viscosity model. Physics of Fluids, 3 (7), 1760-1765.

Hinterberger, C., Fröhlich, J., Rodi, W. 2007. Three-dimensional and depth-averaged Large-Eddy Simulations of some shallow water flows, J. of Hydraulic Engineering, 133, 857-872.

Hinterberger, C., Fröhlich, J., Rodi, W. 2008. 2D and 3D turbulent fluctuations in open channel flow with $Re\tau$ = 590 studied by Large Eddy Simulations. Flow, Turbulence and Combustion, 80, 225-253.

Koken, M., Constantinescu, G. 2008. An investigation of the flow and scour mechanism around isolated spur dikes in a shallow open channel: 2. Conditions corresponding to the final stages of the erosion and deposition process. Water Resources Research, 44, W08407.

Miyawaki, S. 2009. Numerical investigation of scalar transport at a river confluence. CD-ROM Proceedings of the 23rd IAHR Congress, Vancouver.

Miyawaki, S., Constantinescu, G., Rhoads, B., Sukhodolov, A. 2010. On the three-dimensional flow structure at a river confluence with a high momentum ratio. Proc. River Flow 2010, Braunschweig, Germany.

Moser, R.D., Kim, J., Mansour, N.N. 1999. Direct Numerical Simulation of turbulent channel flow up to $Re\tau$ = 590. Phys. Fluids 11, 943-945.

Nezu, I., Nakagawa, A. 1993. Turbulence in open channel flows, IAHR Monograph Series, Balkema, Rotterdam.

Nezu, I., Rodi, W. 1986. Open-channel flow measurements with a laser Doppler anemometer. J. Hydraulic Engineering 112, 335-355.

Piomelli, U., Chasnov, J. 1996. Large-Eddy Simulations: theory and applications, in: Turbulence and Transition Modelling, M. Hallbäck et al. (eds.). Kluwer Academic, 269-331.

Polatel, C. 2006. Large-scale roughness effect on free-surface and bulk flow characteristics in open-channel flows. PhD thesis, Iowa Institute of Hydraulic Research.

Procrajac, D. 2005. Personal communication.

Rhoads, B.L., Sukhodolov, A.N. 2001. Field investigation of three-dimensional flow structure at stream confluences: 1. Thermal mixing and time-averaged velocities. Water Resources Res., 37, 2393-2410.

Rhoads, B.L., Sukhodolov, A.N. 2008. Lateral momentum flux and spatial evolution of flow within a confluence mixing interface. Water Resources Res., 44, WR08440.

Spalart, P. 2009. Detached eddy simulations. Annual Review of Fluid Mechanics, 41, 181-202.

Spalart, P.R., Jou, H.W., Strelets, M., Allmaras, S.R. 1997. Comments on the feasibility of LES for wings, and on a hybrid RANS/LES approach. In : Advances in LES/DNS, Liu, C., Liu, Z. (eds). Greyden Press, Louisiana Tech University, Louisiana, USA.

Stoesser, T., Fröhlich, J., Rodi, W. 2007. Turbulent open-channel flow over a permeable bed. Proc. 32nd IAHR Congress, Venice.

Stoesser, T., Braun, C., Garcia-Villalba, M. Rodi, W. 2008. Turbulent structures in flow over two-dimensional dunes. J. of Hydraulic Engineering, 143, 42-55.

Weitbrecht, V., Sokolofsky, S.A., Jirka, G.H. 2008. Experiments on mass exchange between groin fields and main stream in rivers. J. of Hydraulic Engineering. 134, 173-183.